Direction-Based *P* wave Traveltime Residual Estimation for some Stations Around Southern Thailand, Peninsular Malaysia, Singapore and Sumatra Using a New Ray Tracing Algorithm

A. U. Osagie[1] and I. A. Abir[2]

[1] University of Abuja, Nigeria.

[2] Universiti Sains Malaysia, Malaysia.

Corresponding author: Abel U. Osagie abel.osagie@uniabuja.edu.ng

Key Points:

- This study used 82,325 first-arrival *p* waves from 15,212 earthquakes spanning over five decades from two data centers.
- A newly developed algorithm is used to compute traveltimes and raypaths. Residuals are plotted on a back-azimuth versus epicentral distance.
- The residual values are separated into four back-azimuthal directions. The average values are estimated for each station in the directions.

Abstract

Path dependent corrections relative to traveltimes have been demonstrated to improve event locations. Using available global velocity models, direction-based station corrections can be estimated in a region without calibration data. In this study, traveltime corrections have been obtained for 117 broadband seismic stations around southern Thailand, Peninsular Malaysia, Singapore and Sumatra region of Indonesia. A total of 82,325 first-arrival *p* waves are obtained from 15,212 earthquakes that have occurred around the Sumatra Subduction Zone over five decades (1964 – 2018). The dataset is a combination of arrival time data from the Bulletin of International Seismological Centre and waveforms from the Incorporated Research Institutions for Seismology. A newly developed algorithm for three-dimensional ray tracing is used to compute traveltimes and raypaths. The corrections are based on the IASP91/AK135 velocity models at four back-azimuthal directions. The estimated residuals in seconds (s) ranges from -2.15 to 2.25 s for stations distributed around southern Thailand and a range of -0.76 to 1.60 s for stations within Peninsular Malaysia. A range of 0.59 to 1.08 s for stations within Singapore and -1.52 to 2.46 s for stations distributed around Sumatra (in Indonesia). Station PSI in Sumatra Island recorded the highest number with 4877 arrivals. Stations LEM, KLM and KGM show consistent high residual values at all calculated angles and distances. The result of this study will support routine location of hypocentral parameters within the region. The scheme is being implemented for use in the forward computational process of seismic tomographic inversion in the study area.

Plain Language Summary

Earthquake locations is usually announced after occurrence. These earthquakes release seismic *p* waves which are the first to arrive at seismic stations with known locations. Seismologists determine the location of earthquakes by using an arbitrary velocity model of the earth's subsurface. With many earthquakes, it is sometimes helpful to make create a table with specific time associated with each station in order to improve earthquake locations. This adjustment is called station correction. This paper attempts to determine corrections for 117 stations distributed around southern Thailand, Peninsular Malaysia, Singapore and Sumatra region of Indonesia. To do so, a total of 82,325 first-arrival *P* waves are obtained from 15,212 earthquakes that have occurred around the Sumatra Subduction Zone over five decades (1964 – 2018). The idea is to calculate traveltime residuals (in seconds) based on the bearing of the earthquake to the station (divided into four quadrants). The average residual is estimated for each quadrant and for each station. This is expected to improve the location of earthquakes around the stations.

1 Introduction

Precise location of earthquakes continues to be among the main objectives of seismology. This helps to make good inferences about the subsurface structures responsible for the observed seismicity. Knowledge of the subsurface brings many other benefits which may include economic (in mineral exploration) and safety (in engineering designs). Unfortunately, events with smaller magnitudes at regional distances are usually recorded by fewer stations around the region. Besides, the precision of locations is affected by limitations imposed by other factors like, data quality, the velocity model and the algorithm used for locating the events. There are usually tradeoffs between earthquake locations and velocity model. Fortunately, technological advances have improved the quality of seismic data and different algorithms have been developed to increase the reliability of event locations. However, information about near-surface velocity structures at local/regional distances is not common knowledge.

Global one-dimensional (1-D) reference velocity models like PREM (Dziewonski & Anderson, 1981), IASP91 (Kennett &Engdahl, 1991) and AK135 (Kennett et al., 1995) are good approximations for the purpose of locating hypocentral parameters. However, these approximations may not satisfy velocity variations at local and regional distances. This is due to lateral variations in the crustal and upper mantle which cause deviations in predicted raypaths. The raypath deviation can introduce errors in traveltime calculations. The Group of Scientific Experts' Third Technical Test (GSETT3) has adopted the IASPEI91 (Kennett and Engdahl, 1991) model as the reference traveltime set since 1st January, 1995 (Yang et al.,2001). The IASPEI91 traveltimes can deviate considerably from true traveltimes at regional distances. The deviation in traveltime and raypath can be as much as 2 seconds and 100 km respectively (Bijwaard & Spakman 2000), and as much as 3.9 seconds and 77 km respectively (Zhao & Lei, 2004).

The effect of lateral heterogeneity can be reduced, either by, (1) using regional velocity model or by, (2) applying traveltime corrections to known models for event locations (Yang, et al., 2001). The former requires the development of improved velocity models of the crust and mantle for better prediction of seismic traveltimes (e.g., Villaseñor et al., 2003) while the latter applies traveltime corrections based on the residuals observed for calibration events of known locations (Shearer, 2001). Station corrections e.g., the Source-Specific Station Correction (SSSC) may be required to account for the effects of lateral heterogeneity at a given seismic station. These model-predicted SSSC's may be obtained by ray tracing techniques through the model from each station to points on a specified latitude-longitude grid within specified distances from the station (Villaseñor et al., 2003). Station corrections can be constructed in regions (e.g., with frequent earthquakes and/or explosions) to obtain good calibration data. Regional SSSCs for International Monitoring System (IMS) stations have been developed. Path dependent corrections relative to the IASPEI91 traveltimes have been demonstrated to improve event locations (e.g., Yang et al., 2001). Unfortunately, many regions around the globe do not have calibration data. Hence, station correction may be estimated using available regional and/or global velocity models.

The objective of this research is to estimate the average traveltime residual values (A$\bar{R}$) based on back-azimuth (θ) for regional first-arrival *p* phases up to 10 degrees (^{o}) epicentral distances (Δ) for some stations distributed around the southern part of Thailand, Peninsular Malaysia, Singapore and the Sumatra region of Indonesia. To achieve the objective, a new algorithm capable of ray tracing in 1-D/3-D models is developed to compute traveltimes and raypaths at local and regional distances. The algorithm can use any global 1-D velocity model as reference to create a 3-D model and calculate raypaths and traveltimes within the model. Perturbations can also be carried out within the scheme for tomographic purposes. Calculations of traveltime residual values ($\bar{R}$) for stations are based on θ in four quadrants: NE ($\theta \leq 90^o$), SE ($90^o < \theta \leq 180^o$), SW ($180^o < \theta \leq 270^o$) and NW ($270^o < \theta \leq 360^o$) directions. For validation, the overall calculated A$\bar{R}$ are compared with the published results from the Bulletin of International Seismological Center (BISC). Traveltimes computed with the scheme for hand-picked waveforms from the Incorporated Research Institutions for Seismology (IRIS) are also validated by the results obtained from the TauP Toolkit software (Crotwell et al., 1999) for the same velocity model, hypocenters and station distribution. Station corrections determined in this work are based on the IASP91 model which can also be used for the AK135 model since both models are similar at the crust and upper mantle.

2 Materials and Methods

2.1 The Study Region

The study region encompasses the Sumatran Fault System (SFS) which runs parallel to the Sumatra Subduction Zone (SSZ) where the Indo-Australia plate subducts beneath the Burma microplate and Sunda Block (Amalfi et al., 2016). The predominant tectonic structures in the area are the SSZ and the SFS. Some authors (e.g., Irsyam et al., 2008; Lin et al., 2009) have reported that the SFS consist of 19 segments. The segments are separated by dilatational and contractional step-overs and abrupt changes in trend (Sieh & Natawidjaja, 2000). A total of 117 seismic stations recorded 15 or more earthquakes within the window of events used in this study. The seismic stations are distributed around the southern part of Thailand, Peninsular Malaysia, Singapore and the Island of Sumatra (Indonesia). The station distribution spans latitudes 10º N – 11º S and longitudes 93º E – 115º E and the earthquake epicenters are distributed over an area ~ 1,970,000 km^2 which is roughly the size of Mexico (Fig. 1a and 1b).

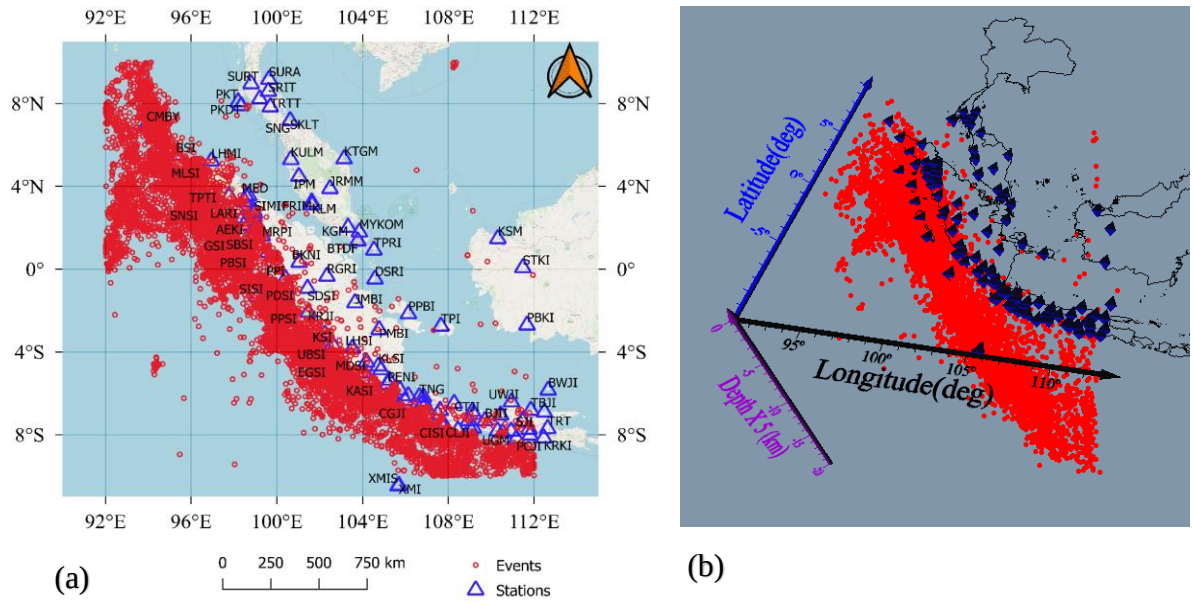

Figure 1. Distribution of 15,176 earthquakes and 117 seismic stations across the region. (a) epicenters (red circles) and seismic stations (blue hollow triangles) and (b) hypocenters (red circles) and seismic stations (blue solid triangles).

Phase picking from the IRIS waveforms is done with the SEISAN software (Havskov & Ottemoller 1999). The corresponding S-file from SEISAN is added to the BISC dataset. A new scheme (CONVT) developed in this study reads the combined file formats. The scheme operates within certain conditions which are predefined by the user (e.g., the limiting boundaries of the study area, the maximum depth of events, maximum epicentral distance and the residual limits). If the limiting boundaries of the study area are not set, CONVT will extract the limits from the largest and smallest values of latitudes and longitudes of the station list. Both the BISC dataset and the IRIS summary file formats can be converted into S-file format for entry into SEISAN

software. Since waveforms can be registered into SEISAN database, this conversion will be useful to validate reported arrivals from the waveforms in the SEISAN database. The routine extracts the number of stations with arrival time data and the combined dataset is converted to input format for a ray tracing algorithm (TRAVT) also developed in this study.

The ray tracing algorithm (TRAVT) is used to compute raypaths and traveltimes. The reported hypocentral parameters from both the BISC and the IRIS are used in this study. First, the station coordinates, the selected 1-D velocity model and the dataset are initiated within TRAVT. Then, a 3-D grid model is constructed from the selected 1-D velocity model using the parameterization technique introduced by Zhao et al. (1992). This technique has been used for tomographic studies (e.g., Zhao, 2012; Wang et al., 2017). Using the haversine formula, the epicentral distance is determined. The hypocentral distance and azimuth are also determined within TRAVT. The take-off angle for up-going rays from the source are determined by a subroutine (TRAYD) using the technique introduced by Kim and Baag (2002) that relates the take-off angle at the source to the horizontal distances covered by the seismic wave (Fig. 2a). This two-point ray shooting technique has been used by some authors (e.g., Kang & Kim, 2013; Osagie & Kim, 2013; Hong et al., 2017; Osagie, et al, 2017). Another subroutine (TRAYR) computes raypaths and traveltimes for refracted rays from all existing boundaries in the model. The ray with the shortest traveltime from the result of TRAYD and TRAYR is selected and the wave type is determined within TRAVT.

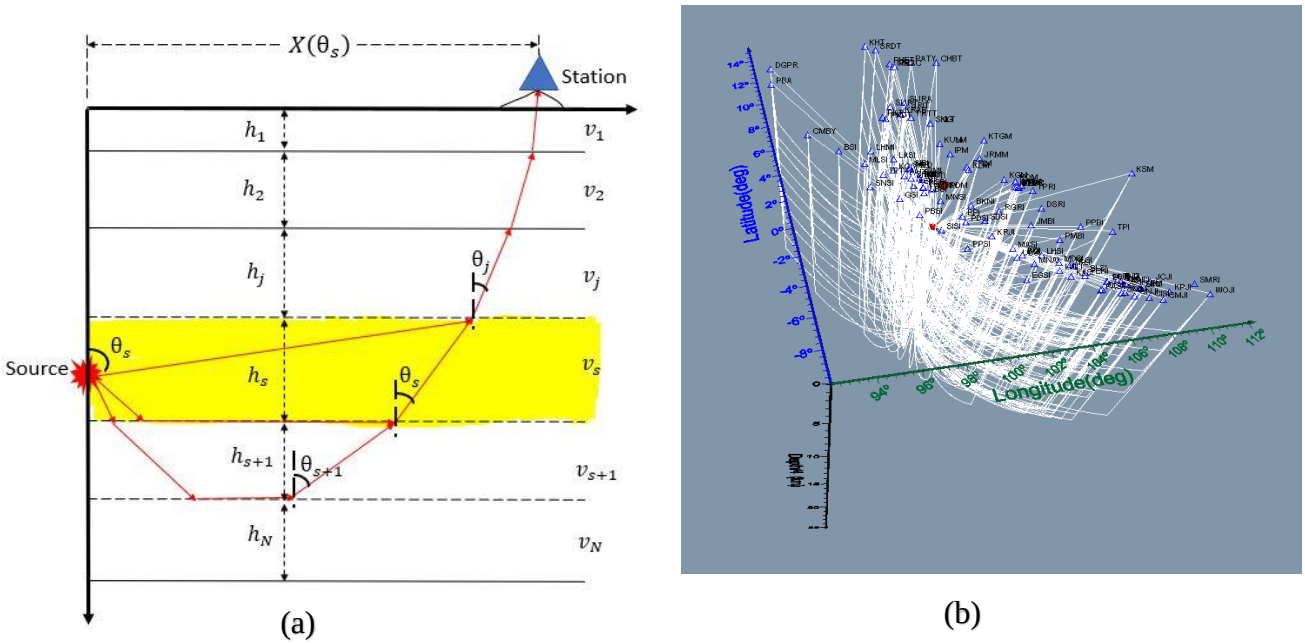

Figure 2 (a) A schematic diagram showing raypaths (red arrow lines) for both direct and refracted rays in an N-layered model with the thicknesses h_j and velocities v_j. The source is at the layer with thickness h_s and velocity v_s and the station (blue triangle) is at some elevation. (b) Raypaths (white lines) from three sources (red sphere) to stations (blue triangles) for a 10-layer test model. The depth axis of (2b) is 55 times exaggerated.

The computed rays are constrained to bottom in each layer between interfaces and might be reflected off the top of the layer or turn within the layer to retain raypath with the shortest traveltime. Apart from boundary values, the various points are determined by a predefined value of step-length as the rays propagate from source to stations. A variable is defined that carries

information (latitude, longitude, depth, velocity, time from source, raypath length from source, angle ray makes the vertical) at various points along the path step-length between source and station. For refracted wave the variable index the boundary of refraction. The depth of refraction for any boundary are adjustable within the scheme. TRAVT has the advantage of rapid convergence resulting in less computational time and resources. The scheme can accommodate a model with as many layers as required for computing traveltimes for local and regional investigation of the sub-surface. This can be useful for both field seismic investigations, generation of synthetic seismograms, determination of refraction depths and to estimate crustal thicknesses/Moho depths. It can also be used for the forward calculation process of tomographic inversions and has been successfully integrated into a tomographic scheme. The ability of the ray tracing scheme to identify boundaries of refraction has been demonstrated with a fictitious 10-layer test-model (Fig. 2b). Note that the depth axis is 55 times exaggerated compared with the dimensions of the longitude and latitude axes.

3 Data

Earthquakes (magnitude > 3.5 mb) used in this study spans latitudes 10º N – 10º S and longitudes 92º E–114º E are confined to the top 100 km in focal depths. This selection is due to the intention of the authors to carry out tomographic inversion of the area in the near future. The data is obtained from two sources: (1) waveforms from Incorporated Research Institutions for Seismology (IRIS) and (2) arrival time dataset from the Bulletin of International Seismological Center (BISC). A software (JWEED) developed by Seismology Department at the University of South Carolina (USC, 2012) is used to retrieve waveforms from the IRIS online free access archive for the period between the year 2006 and 2018. This was the period of good waveform data during the time of data collection in 2018. In 2018, this study also obtained all available arrival time data from BISC between 1964 and 2016. The BISC data ended in 2016 as at the time of data collection for this study. Review of the BISC data is usually about 24 months behind time because arrival times are manually checked by BISC analysts (ISC, 2019). Later in 2019, the revised BISC dataset until mid-2017 was added to the dataset. Picked phases from the IRIS waveforms are combined with the dataset from the BISC to obtain a total of 15,212 events. The combined dataset contains 82,325 are *P* wave first arrivals.

4 Results and Discussion

After the ray tracing scheme (TRAVT) has been validated with a test-model, traveltimes and raypaths are computed using the IASP91 velocity model. The computed traveltime result of manual picks from the IRIS waveforms are validated by the TauP Toolkit software for the same velocity model, hypocenters and station distribution around the study area. The flowchart (Fig. 3) shows the process from data collection, preparation, analysis and computation. Raypaths for P_g and P_n phases calculated using the IASP91 model and station locations are shown in figure 4. (note that the depth axis is 55 times exaggerated).

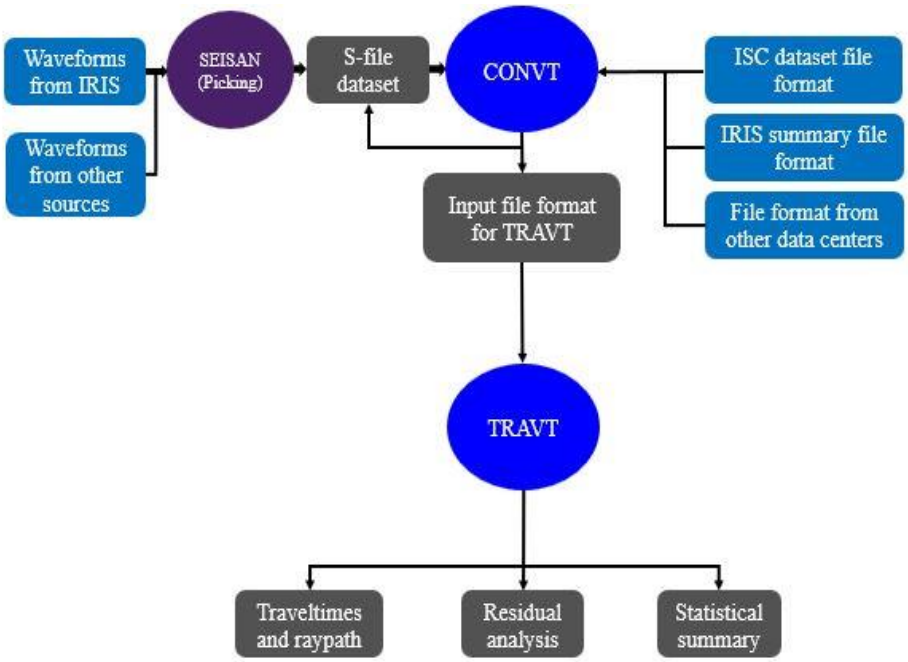

Figure 3 Flowchart of data collection, analysis and computation (blue circles are the algorithms)

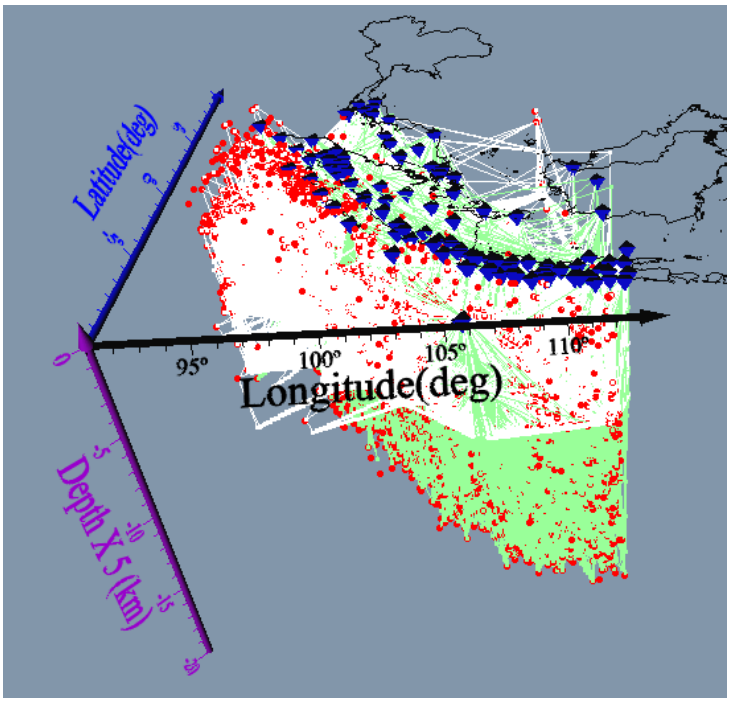

Figure 4 Some Ray path for P_g and P_n phase calculated using the IASP91 model (depth axis is 55 times exaggerated). Red circles represent earthquake locations while blue triangles represent seismic stations. Green lines are direct raypaths and while lines are refracted raypaths.

The number of arrivals recorded by the stations range from 15 (MBSI) to 4877 (PSI). The traveltime residuals are compared with the published result from the BISC for the same "Event

ID" and "Arrival ID". The ℟ values are represented on a plot of θ against Δ for some selected stations which are arranged according to country and in decreasing number of arrivals (Fig. 5).

The stations at the northern end of this spectrum are within the southern part of Thailand. Arranged in order decreasing number of recorded arrivals are: SNG, TRTT, PKDT, SKLT, SRIT, SURT, SURA, KRAB and PKT. Station SNG indicate a relatively positive ℟ values (Fig. 5a). TRTT and PKDT show similar negative ℟ for $\Delta > 750$ km (Fig. 5b and 5c). SKLT indicates a slightly more positive ℟ values for events between 500 - 750 km away and θ between 180º – 270º (Fig. 5d).

The ten stations within Peninsular Malaysia include: KULM, IPM, MYKOM, KGM, FRIM, KTGM, DSRI, KLM, JRMM, and KSM. Station KTGM is on the east coast of the Peninsula while the rest are on the west and central part of the Peninsula. Heterogeneity appears to be present when seismic waves travel toward stations KULM and IPM (Fig. 5e and 5f) respectively. A consistently positive ℟ values is observed for stations KGM and KLM (Fig. 5g and 5h) respectively, suggesting the presence of low velocity region with respect to the IASP91 model in the SW direction from the stations. Stations KOM and KUM (IRIS station code names) are observed to be the same as stations MYKOM and KULM respectively on the BISC station list.

At the southernmost end of the Peninsula is Singapore with four stations: BTDF, BESC, NTU and KAPK. While station BTDF is on the BISC list, the other stations (BESC, NTU and KAPK) are only on the IRIS station list and appeared only on the hand-picked data. This is responsible for the fewer arrivals recorded for these stations. However, there appears to be a common trend in the observed velocity heterogeneities among the stations. Examples are shown for BTDF and BESC (Fig. 5i and 5j) respectively.

The two southernmost stations (XMI and XMIS) are situated in Christmas Island, Australia while the easternmost station (CMBY) is located in the Andaman Islands, India. The two Australian stations (Fig. 5k and 5l) show mild and similar heterogeneities. CIMB (Fig. 5m) changes from slightly positive to negative ℟ values when Δ is beyond 400 km.

Most stations used in this study are distributed around the Island of Sumatra in Indonesia. The stations show varying degrees of heterogeneities. Station PSI (Fig. 5n) recorded the highest number with 4877 arrivals. There is a consistent positive ℟ values for $\theta > 250$º. However, the station shows a strong negative ℟ values for $\Delta > 800$ km and $\theta < 270$º. GSI (Fig. 5o) shows some slight similarities with PSI in ℟ for $\Delta > 800$ km. Other stations within the Sumatra region show varying degrees of heterogeneities (e.g., Fig. 5p – 5t). Station LEM (Fig. 5t) shows consistent positive ℟ values at all θ, which suggest the presence of a low velocity structure around the station.

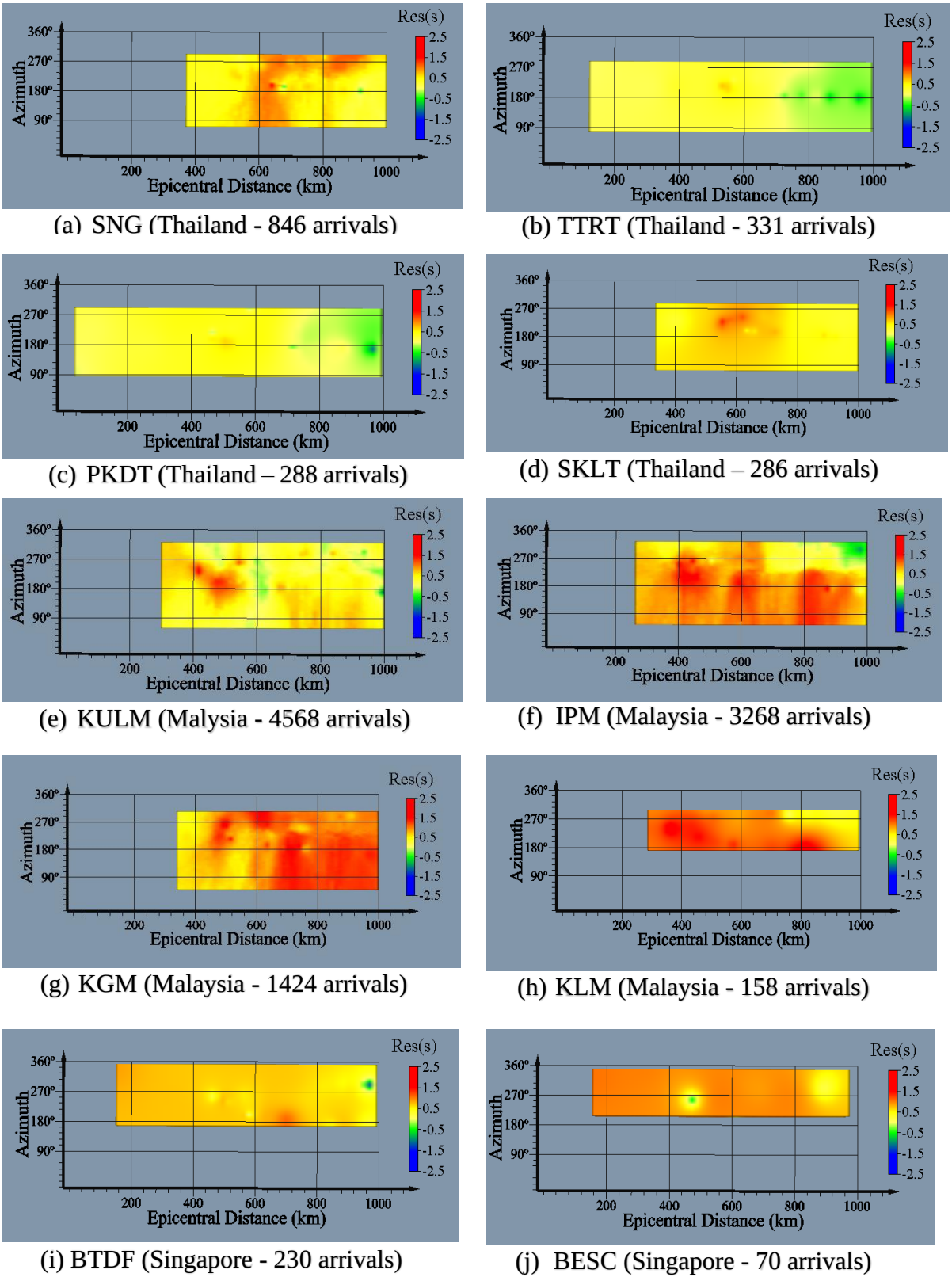

(a) SNG (Thailand - 846 arrivals)

(b) TTRT (Thailand - 331 arrivals)

(c) PKDT (Thailand – 288 arrivals)

(d) SKLT (Thailand – 286 arrivals)

(e) KULM (Malysia - 4568 arrivals)

(f) IPM (Malaysia - 3268 arrivals)

(g) KGM (Malaysia - 1424 arrivals)

(h) KLM (Malaysia - 158 arrivals)

(i) BTDF (Singapore - 230 arrivals)

(j) BESC (Singapore - 70 arrivals)

Figure 5 Plot of back-azimuth against epicentral distance for some stations within the study region. The figures are arranged according to county and in decreasing order of arrivals.

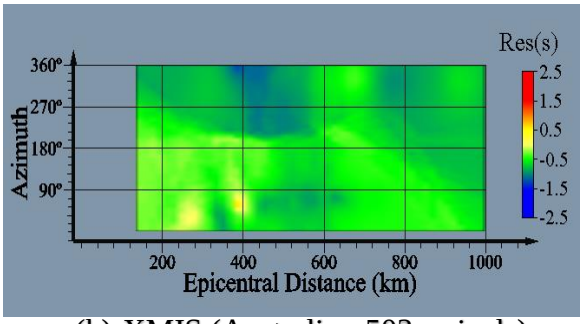

(k) XMIS (Australia - 503 arrivals)

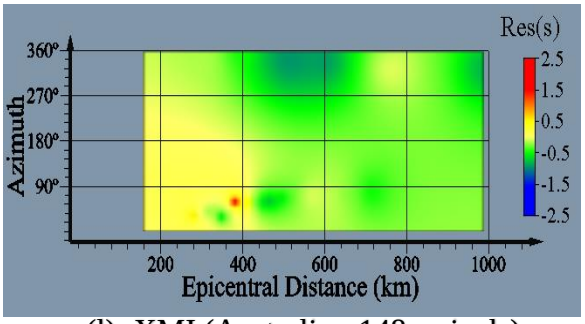

(l) XMI (Australia - 148 arrivals)

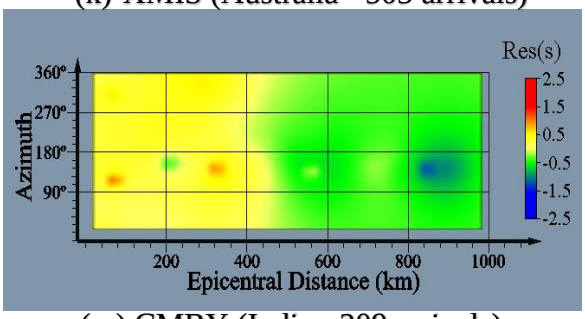

(m) CMBY (India - 209 arrivals)

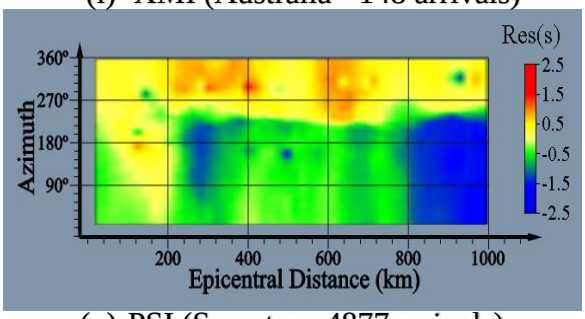

(n) PSI (Sumatra - 4877 arrivals)

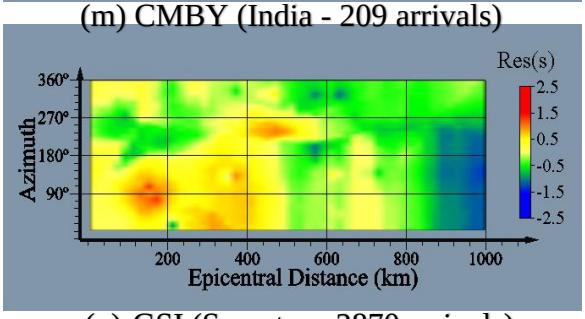

(o) GSI (Sumatra - 2870 arrivals)

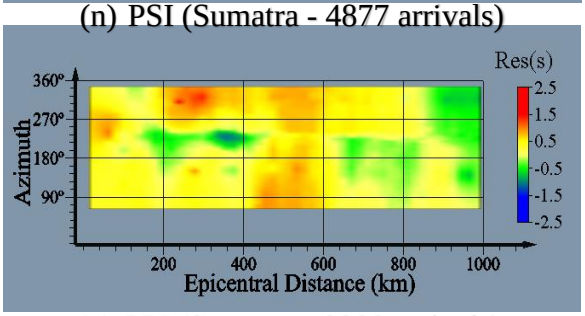

(p) PPI (Sumatra - 2299 arrivals)

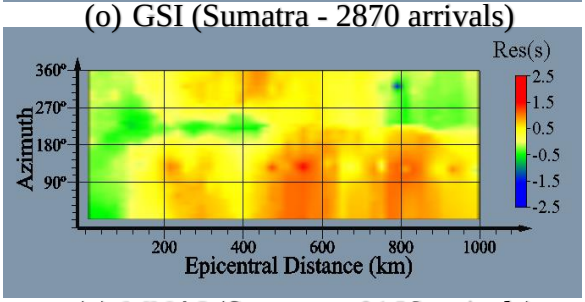

(q) MNAI (Sumatra - 2156 arrivals)

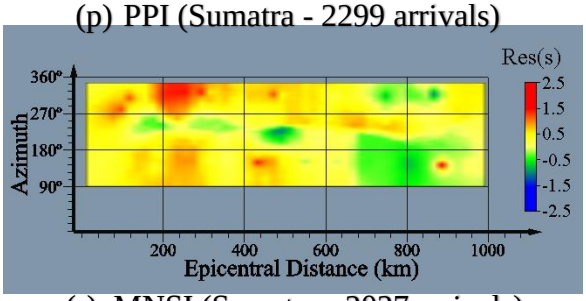

(r) MNSI (Sumatra - 2027 arrivals)

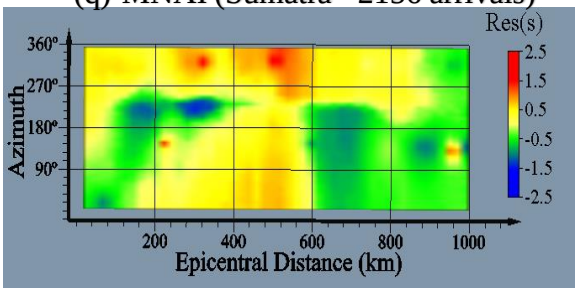

(s) PDSI (Sumatra - 1790 arrivals)

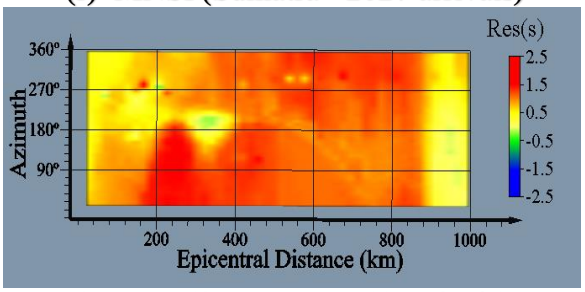

(t) LEM (Sumatra - 1740 arrivals)

Figure 5 continues

Table 1 Calculated (AR̄) from four back-azimuthal directions (columns 8 - 11). Columns 12 and 13 are the overall calculated (AR̄) and BISC (AR̄) respectively for 117 stations distributed around the region. The stations are arranged according to country and in decreasing number of arrivals

Sn	Stn Code	Lat [deg]	Lon [deg]	Z [km]	Country	NArv	$\theta \leq 90^o$	$90^o < \theta \leq 180^o$	$180^o < \theta \leq 270^o$	$270^o < \theta \leq 360^o$	AR̄ -Cal [s]	AR̄-ISC [s]
1	XMIS	-10.4807	105.6519	0.2430	Australia	503	-0.29	0.00	0.00	-0.86	-0.47	-0.64
2	XMI	-10.4495	105.6895	0.2780	Australia	148	0.04	0.00	0.00	-0.78	-0.13	-0.17
3	CMBY	7.0109	93.9266	0.0100	India	209	0.08	-0.14	-0.26	0.73	-0.04	-0.18
4	PSI	2.8010	98.9240	0.9870	Indonesia	4877	0.15	-0.71	0.01	0.87	0.11	-0.08
5	GSI	1.3039	97.5755	0.1070	Indonesia	2870	0.56	-0.18	0.09	0.26	0.09	-0.13
6	PPI	-0.4568	100.3970	0.0000	Indonesia	2299	-0.14	0.23	0.03	0.57	0.29	0.12
7	MNAI	-4.3605	102.9557	0.1540	Indonesia	2156	0.08	0.50	0.04	0.31	0.32	0.15
8	MNSI	0.7955	99.5796	0.0000	Indonesia	2027	0.00	0.00	0.15	0.71	0.42	0.22
9	PDSI	-0.9118	100.4617	0.2760	Indonesia	1790	-0.08	-0.11	-0.34	0.40	0.02	-0.13
10	LEM	-6.8266	107.6175	1.2930	Indonesia	1740	0.96	0.99	0.79	1.04	0.96	0.77
11	KASI	-5.5236	104.4967	0.0000	Indonesia	1720	0.22	0.55	-0.36	0.29	0.24	0.05
12	MDSI	-4.4861	104.1783	0.0000	Indonesia	1685	0.00	0.76	0.42	0.56	0.57	0.39
13	LHMI	5.2288	96.9472	0.0030	Indonesia	1673	-0.09	0.30	0.51	0.48	0.46	0.29
14	BKNI	0.3262	101.0396	0.0650	Indonesia	1608	-0.18	0.30	0.46	0.60	0.49	0.34
15	SISI	-1.3265	99.0895	0.0000	Indonesia	1569	0.59	-0.15	-0.05	0.23	0.06	-0.10
16	KSI	-3.6517	102.5929	0.5390	Indonesia	1539	-0.86	0.34	0.07	0.49	0.34	0.21
17	LWLI	-5.0175	104.0589	0.9380	Indonesia	1533	0.71	0.87	0.15	0.62	0.57	0.38
18	TPTI	3.2600	97.1800	0.0090	Indonesia	1456	0.44	0.11	-0.30	0.30	-0.05	-0.29
19	KCSI	3.5220	97.7715	0.2050	Indonesia	1369	0.97	0.18	0.53	0.98	0.52	0.25
20	CISI	-7.5557	107.8153	0.5440	Indonesia	1349	0.68	0.23	-0.30	-0.24	-0.14	-0.41
21	TSI	3.5008	98.5645	0.0000	Indonesia	1335	-0.19	0.59	0.84	0.88	0.80	0.61
22	UGM	-7.9125	110.5231	0.3500	Indonesia	1208	0.65	0.31	0.13	0.69	0.41	0.13
23	PPSI	-2.7630	100.0096	0.0000	Indonesia	1204	0.24	0.27	-0.82	0.08	0.08	-0.03
24	CGJI	-6.6135	105.6929	0.0000	Indonesia	1143	-1.26	0.36	-0.33	-0.29	-0.08	-0.30
25	SDSI	-0.9324	101.4282	0.0000	Indonesia	1038	0.00	0.66	0.39	0.84	0.58	0.41
26	KLI	-4.8630	104.8567	0.0320	Indonesia	950	0.37	0.93	0.70	0.85	0.82	0.62
27	MLSI	4.2668	96.4040	0.0580	Indonesia	932	-0.19	0.09	0.30	0.22	0.20	-0.02
28	MASI	-3.1415	102.2396	0.3840	Indonesia	922	-0.34	0.87	0.21	0.67	0.60	0.42
29	CNJI	-7.3090	107.1296	0.0000	Indonesia	916	-0.02	0.34	-0.23	-0.30	-0.06	-0.33
30	SKJI	-7.0053	106.5563	0.1000	Indonesia	863	0.41	0.51	-0.30	0.38	0.31	0.05
31	BSI	5.4964	95.2961	0.1920	Indonesia	839	-1.17	-0.51	-0.07	-0.21	-0.36	-0.51
32	LHSI	-3.8267	103.5233	0.0000	Indonesia	831	-1.28	1.09	0.69	0.91	0.87	0.71
33	DBJI	-6.5538	106.7497	0.2110	Indonesia	827	0.31	0.91	0.45	0.62	0.65	0.40
34	SNSI	2.4089	96.3267	0.0140	Indonesia	808	1.00	0.22	0.26	0.10	0.22	-0.09
35	CMJI	-7.7837	108.4485	0.0000	Indonesia	760	-0.08	0.19	-0.12	0.13	0.07	-0.21
36	PBSI	-0.0547	98.2800	0.0000	Indonesia	756	0.59	0.24	0.08	0.43	0.37	0.09
37	PWJI	-8.0220	111.8039	0.0000	Indonesia	750	0.35	0.01	0.41	0.85	0.58	0.25
38	RPSI	2.6951	98.9240	0.0000	Indonesia	743	-1.35	-0.21	0.63	0.74	0.55	0.37

248 **Table 1** continues
249

Sn	Stn Code	Lat [deg]	Lon [deg]	Z [km]	Country	NArv	θ ≤ 90º	90º < θ ≤ 180º	180º < θ ≤ 270º	270º < θ ≤ 360º	AR -Cal [s]	AR-ISC [s]
39	SBJI	-6.1200	106.1300	0.0000	Indonesia	698	0.25	0.87	0.19	0.73	0.59	0.36
40	PCJI	-8.1947	111.1771	0.0000	Indonesia	693	-0.04	-0.47	0.28	0.60	0.38	0.07
41	BLSI	-5.3676	105.2452	0.1470	Indonesia	691	1.99	0.61	0.40	1.04	0.66	0.41
42	PPBI	-2.1616	106.1364	0.0640	Indonesia	676	-1.14	1.25	0.85	1.14	0.94	0.85
43	KRJI	-2.0912	101.4619	0.8110	Indonesia	671	0.00	0.69	0.24	0.83	0.59	0.41
44	KLSI	-4.6900	104.7300	0.0810	Indonesia	648	-1.52	0.82	0.68	0.92	0.82	0.64
45	SMRI	-7.0491	110.4407	0.2030	Indonesia	626	0.10	0.94	1.12	0.72	1.01	0.77
46	RGRI	-0.3491	102.3338	0.0410	Indonesia	608	0.00	0.98	0.75	0.66	0.76	0.64
47	TNG	-6.1717	106.6462	0.0140	Indonesia	584	0.15	1.10	0.75	0.76	0.83	0.47
48	TPI	-2.7563	107.6534	0.0250	Indonesia	536	-0.29	1.06	0.69	0.81	0.75	0.62
49	KPJI	-7.3330	108.9310	0.0000	Indonesia	533	1.19	1.12	0.98	1.18	1.07	0.77
50	PMBI	-2.9270	104.7720	0.0300	Indonesia	512	0.23	0.75	0.40	0.21	0.41	0.28
51	PENI	-5.5667	105.1710	0.2000	Indonesia	449	-0.48	0.70	0.86	1.22	0.98	0.19
52	KALI	-7.1064	106.6590	0.8100	Indonesia	366	0.13	0.41	0.09	0.54	0.49	-0.65
53	TPRI	0.9184	104.5263	0.0410	Indonesia	366	0.00	0.88	0.81	1.07	0.85	0.80
54	JMBI	-1.6335	103.6417	0.0000	Indonesia	364	0.00	1.20	0.82	0.94	0.86	0.76
55	PASI	-6.6894	105.5890	0.2200	Indonesia	347	1.28	0.39	-0.52	0.26	0.24	-0.49
56	WOJI	-7.8372	110.9236	0.0000	Indonesia	345	-0.10	0.14	0.28	1.01	0.46	0.17
57	YOGI	-7.8166	110.2949	0.1600	Indonesia	335	0.85	0.05	0.14	0.46	0.21	-0.01
58	CBJI	-6.4200	106.8500	0.0000	Indonesia	321	-1.18	-0.88	0.33	1.62	0.58	0.25
59	BJII	-7.3329	109.7096	0.6290	Indonesia	309	0.00	0.41	0.33	0.92	0.46	0.34
60	LARI	2.8856	98.1572	0.8200	Indonesia	285	0.00	0.24	0.28	0.99	0.46	-0.64
61	PULI	-6.3450	105.9760	1.3460	Indonesia	285	1.77	0.95	0.02	1.09	0.93	0.21
62	SJI	-7.7349	111.7669	0.7230	Indonesia	276	1.12	0.54	0.71	0.87	0.75	0.45
63	JCJI	-6.4900	108.2700	0.0000	Indonesia	270	1.22	-0.75	-0.36	1.34	-0.08	-0.33
64	GRJI	-6.9145	112.4793	0.0000	Indonesia	249	0.00	0.00	1.03	1.49	1.07	0.79
65	SINI	-7.0144	107.5000	1.0000	Indonesia	249	-1.46	0.83	0.55	0.87	0.78	0.35
66	MRPI	1.6125	99.3172	1.1000	Indonesia	230	-0.47	0.81	0.62	1.06	0.82	-0.30
67	PACI	-6.5928	106.9100	0.8500	Indonesia	228	2.46	1.01	0.69	1.08	0.97	0.58
68	TRT	-7.7040	112.6350	0.0000	Indonesia	228	0.00	0.00	0.68	0.99	0.79	0.47
69	AEKI	2.1017	98.4536	0.8400	Indonesia	219	0.00	0.03	0.05	0.43	0.17	-0.64
70	SIBI	3.2408	98.5044	2.0500	Indonesia	169	0.00	0.96	1.15	0.93	1.01	0.30
71	UWJI	-6.4191	110.9474	0.0620	Indonesia	165	0.00	0.65	0.89	1.32	0.90	0.68
72	NGJI	-7.3676	111.4612	0.0000	Indonesia	164	1.96	0.99	1.34	1.17	1.28	1.01
73	PCBI	1.8900	98.9253	1.0000	Indonesia	162	-0.13	-0.09	0.03	0.41	0.15	0.04
74	KRKI	-8.1583	112.4525	0.0000	Indonesia	142	0.00	0.00	0.62	1.11	0.77	0.49
75	TBJI	-6.8179	111.8481	0.0000	Indonesia	140	0.00	1.04	0.96	0.70	0.94	0.71
76	SEMI	2.4603	98.3917	1.7500	Indonesia	137	0.07	-0.50	0.17	0.58	0.02	-0.06
77	RBSI	-5.8445	105.7420	0.0000	Indonesia	133	0.00	0.53	-0.33	0.92	0.41	0.24
78	MED	3.5500	98.6833	0.0320	Indonesia	125	0.00	0.70	0.49	0.50	0.56	0.41

Table 1 continues

Sn	Stn Code	Lat [deg]	Lon [deg]	Z [km]	Country	NArv	θ ≤ 90º	90º < θ ≤ 180º	180º < θ ≤ 270º	270º < θ ≤ 360º	AR̄ -Cal [s]	AR̄-ISC [s]
79	TRSI	2.0256	98.9594	0.9790	Indonesia	121	0.00	0.85	0.30	0.58	0.54	0.50
80	DJA	-6.1833	106.8362	0.0080	Indonesia	117	0.00	0.85	0.38	0.25	0.41	0.14
81	EGSI	-5.3526	102.2767	0.0360	Indonesia	108	-0.04	0.56	0.35	-0.20	0.10	-0.12
82	SIMI	2.6889	98.9469	1.6810	Indonesia	107	0.00	0.32	0.76	0.74	0.61	0.39
83	CLJI	-7.7187	109.0150	0.0460	Indonesia	91	0.00	-0.36	0.26	0.52	0.22	-0.03
84	SBSI	1.5500	98.8900	0.1470	Indonesia	90	0.33	-1.29	0.83	0.00	0.14	0.11
85	PBKI	-2.7047	111.6697	0.0740	Indonesia	88	0.00	0.64	0.93	-1.15	0.87	0.94
86	HUTI	2.3153	98.9711	1.6000	Indonesia	84	0.00	0.71	0.78	0.78	0.76	0.48
87	TGJI	-6.8679	109.1210	0.0440	Indonesia	65	0.00	0.12	0.50	2.05	0.60	0.40
88	BWJI	-5.8511	112.6578	0.0580	Indonesia	64	0.00	0.00	0.99	0.10	0.97	0.83
89	BBJI	-7.4626	107.6500	0.6150	Indonesia	55	0.00	0.58	-0.18	-0.04	0.21	0.32
90	CTJI	-7.0075	109.1836	0.1040	Indonesia	42	0.00	1.10	1.22	0.83	1.14	0.83
91	UBSI	-3.7611	102.2714	0.0280	Indonesia	39	0.00	0.24	0.29	1.01	0.50	0.34
92	SCJI	-7.6810	109.1689	0.0450	Indonesia	32	1.57	-0.29	0.76	1.18	0.50	0.18
93	STKI	0.0656	111.4772	0.0880	Indonesia	22	0.00	1.77	1.25	-1.09	1.17	1.29
94	MBSI	-3.7611	102.2710	0.0270	Indonesia	15	0.00	0.64	-0.64	0.49	0.24	0.21
95	KULM	5.2900	100.6500	0.0740	Malaysia	4568	1.60	0.67	0.60	0.33	0.58	-0.11
96	IPM	4.4795	101.0255	0.2470	Malaysia	3268	0.09	1.07	0.74	-0.02	0.58	0.39
97	MYKOM	1.7900	103.8500	0.0000	Malaysia	1528	0.00	0.61	0.69	0.64	0.68	0.61
98	KGM	2.0157	103.3190	0.1030	Malaysia	1424	0.06	1.10	0.97	0.98	0.98	0.78
99	FRIM	3.2370	101.6250	0.0980	Malaysia	722	0.00	0.95	0.63	-0.02	0.57	0.56
100	KTGM	5.3280	103.1340	0.0560	Malaysia	566	0.00	0.00	0.63	0.84	0.63	0.69
101	DSRI	-0.4793	104.5778	0.0580	Malaysia	491	-1.41	1.02	0.80	0.98	0.84	0.78
102	KLM	3.1025	101.6450	0.0460	Malaysia	158	0.00	1.42	1.25	0.08	0.87	0.62
103	JRMM	3.8867	102.4767	0.0720	Malaysia	59	0.00	1.72	1.02	0.04	0.66	0.53
104	KSM	1.4733	110.3083	0.0660	Malaysia	18	0.00	-0.76	0.00	1.25	0.40	-0.22
105	BTDF	1.3608	103.7729	0.0640	Singapore	230	0.00	0.59	0.69	0.75	0.71	0.68
106	BESC	1.3422	103.8513	0.0030	Singapore	70	0.00	0.00	1.08	0.76	0.91	0.91
107	NTU	1.3537	103.6852	0.0050	Singapore	65	0.00	0.00	1.05	0.74	0.89	0.89
108	KAPK	1.2967	103.8883	-0.0290	Singapore	62	0.00	0.00	0.91	0.94	0.92	0.92
109	SNG	7.1770	100.6170	0.0040	Thailand	846	0.26	0.90	0.76	0.83	0.77	-0.05
110	TRTT	7.8362	99.6912	0.0710	Thailand	331	-0.14	0.82	0.02	0.71	0.05	0.01
111	PKDT	7.8920	98.3350	0.0530	Thailand	288	-2.15	0.72	0.17	0.87	0.22	0.15
112	SKLT	7.1700	100.6200	0.0140	Thailand	286	-0.21	0.00	0.58	-0.32	0.54	0.50
113	SRIT	8.5955	99.6020	0.0580	Thailand	231	0.00	0.47	0.31	0.23	0.31	0.22
114	SURT	8.9577	98.7950	0.0260	Thailand	190	0.00	1.07	0.38	0.84	0.41	0.47
115	SURA	9.1663	99.6295	-0.0050	Thailand	110	0.00	1.02	0.48	1.92	0.50	0.56
116	KRAB	8.2215	99.1965	0.0580	Thailand	102	0.00	0.51	0.49	0.87	0.49	0.56
117	PKT	8.0800	98.1900	0.0000	Thailand	25	0.00	1.40	0.50	2.25	0.68	0.51

Station coordinates and the computed AR at the four θ directions (NE, SE, SW and NW) are shown in Table 1. Columns 2 - 13 respectively are: (2) station code, (3) station latitude (deg), (4) station latitude (deg), (5) station elevation (km), (6) Country where station is located, (7) number of arrivals recorded by station, (8) calculated AR (s) in the NE direction of θ, (9) calculated AR (s) in the SE direction of θ, (10) calculated AR (s) in the SW direction of θ, (11) calculated AR (s) in the NW direction of θ, (12) calculated AR (s) in all θ directions and (13) AR (s) from the BISC results.

5 Conclusions

Hypocentral parameters from the bulletin of International Seismological Center and the Incorporated Research Institutions for Seismology are combined to obtain a total of 15,212 earthquakes. The selected earthquake data (magnitude > 3.5 mb) spans five decades and are confined to the top 100 km in focal depths. A total of 117 broadband stations is used to obtain 82,325 first-arrival *P* waves within this window of events. A new algorithm for ray tracing in 1-D/3-D models have been developed and shown to accommodate any model with as many layers to compute traveltimes and raypaths for use in local/regional sub-surface investigations. The scheme has been successfully incorporated for forward calculations in a scheme for 3-D tomographic studies and will be useful for other applications like generating synthetic seismograms. Traveltimes are computed using the IASP91 model to all stations used in this study.

The average residual values at the four back-azimuthal directions (NE, SE, SW and NW) show varying degrees of heterogeneities. The two southernmost stations are in Australia with residual values ranging from -0.86 to -0.29 s. The easternmost station is in India and the values range from -0.14 to 0.73 s. The average residual values range from -2.15 to 2.25s for stations in southern Thailand, -0.76 to 1.60 s for stations in Peninsular Malaysia. Only station BTDF among the four Singaporean stations is listed on the bulletin of International Seismological Center station list. The other three stations (BESC, NTU and KAPK) are listed only in the Incorporated Research Institutions for Seismology station list. The average residual values for the stations in Singapore range from 0.59 to 1.08 s. Most stations used in this study are distributed around the Sumatra region of Indonesia. Their average residual values range from-1.52 and 2.46 s. Station PSI in Sumatra Island recorded the highest number of arrivals. A consistently positive residual values at all calculated angles and distances is observed for stations KLM and KGM located in the western corner of Peninsular Malaysia. This is also the case with station LEM which is locate in Sumatra. The result of this study will support routine location of hypocentral parameters within the region. The algorithm can be useful in generating synthetic seismograms and for the forward computational process of seismic tomographic studies.

Acknowledgments

The authors thank Kim Woohan for the use of his two-point ray tracing codes which was modified in a subroutine within our algorithm. The authors acknowledge the Bulletin of International Seismological Center (ISC) from where part of the arrival time data used in this study is obtained. Also, the facilities of IRIS Data Services were used for access to waveforms and earthquake catalog which form part of the data used in this study. Data used for the study is available at https://data.mendeley.com/drafts/j2c8nmmnzt. The algorithms (CONVT, TRAVT) developed in this study, seismic stations and the figures generated are available at https://data.mendeley.com/drafts/bd82mtfgbc.

References

Amalfi, O., Phil, C., David, R., & Sri, H. (2016). Sensitivity analysis for probabilistic seismic hazard analysis (PSHA) in the Aceh Fault Segment, Indonesia. *Geological Society, London, Special Publications, 441*, 121-131. doi: https://doi.org/10.1144/SP441.5

Bijwaard, H., & Spakman, W. (2000). Non-linear global *P* wave tomography by iterated linearized inversion. *Geophysical Journal International, 141*(1), 71-82.

Crotwell, H. P., Owens, T. J., & Ritsema, J. (1999). The TauP Toolkit: Flexible seismic traveltime and raypath utilities. *Seismological Research Letters, 70*(2), 154-160.

Dziewonski, A. M., & Anderson, D. L. (1981). Preliminary reference Earth model. *25*(4), 297-356.

Havskov, J., & Ottemoller, L. (1999). SEISAN earthquake analysis software. *Seismological Research Letters, 70*(5), 532-534.

Hong, T. K., Lee, J., Kim, W., Hahm, I. K., Woo, N. C., & Park, S. (2017). The 12 September 2016 ML5. 8 midcrustal earthquake in the Korean Peninsula and its seismic implications. *Geophys Res Lett, 44*(7), 3131-3138.

Irsyam, M., Dangkua, D. T., Hoedajanto, D., Hutapea, B. M., Kertapati, E. K., Boen, T., & Petersen, M. D. (2008). Proposed seismic hazard maps of Sumatra and Java islands and microzonation study of Jakarta city, Indonesia. *Journal of earth system science, 117*(2), 865-878.

ISC. (2019). International Seismological Center Bulletin. Retrieved from http://www.isc.ac.uk/

Kang, Y.-A., Kim, W., & Kang, T.-S. J. G. J. (2013). Relocation of earthquakes beneath the East Sea of Korea: uncertainty of hypocentral parameters caused by refracted waves. *17*(2), 173-182.

Kennett, B. L., Engdahl, E. R., & Buland, R. (1995). Constraints on seismic velocities in the Earth from traveltimes. *eophysical Journal International, 122*(1), 108-124.

Kennett, B. L. N., & Engdahl, E. R. (1991). Traveltimes for global earthquake location and phase identification. *Geophysical Journal International, 105*(2), 429-465.

Kim, W., & Baag, C.-E. (2002). Rapid and accurate two-point ray tracing based on a quadratic equation of takeoff angle in layered media with constant or linearly varying velocity functions. *Bull. Seism. Soc. Am, 92*(6), 2251-2263.

Lin, J.-Y., Pichon, X. L., Rangin, C., Sibuet, J.-C., & Maury, T. (2009). Spatial aftershock distribution of the 26 December 2004 great Sumatra-Andaman earthquake in the northern Sumatra area. *Geochem Geophys Geosyst, 10*(2009), 1-15. doi:doi:10.1029/2009GC002454

Osagie, A. U., Nawawi, M., Khalil, A. E., & Abdullah, K. (2017). Regional traveltime residual studies and station correction from 1-D velocity models for some stations around Peninsular Malaysia and Singapore. *NRIAG Journal of Astronomy Geophysics, 6*(1), 19-29.

Osagie, A. U., & Woohan, K. (2013). Relocation of Earthquakes that Occurred Beneath Parkfield Region of California using VELHYPO. *IOSR Journal of Applied Geology and Geophysics, 1*(3), 66-81.

Shearer, P. M. (2001). Improving Global Seismic Event Locations Using Source-Receiver Reciprocity. *Bulletin of the Seismological Society of America, 91*, 594–603.

Sieh, K., & Natawidjaja, D. (2000). Neotectonics of the Sumatran fault, Indonesia. *Journal of Geophysical Research, 105*(B12), 28295-28326.

USC. (2012). JWEED. South Carolina Seismology Department at the University of South Carolina. Retrieved from http://www.seis.sc.edu/software

Villaseñor, A., Barmin, M., Ritzwoller, M., & Levshin, A. (2003). Computation of regional travel times and station corrections from three-dimensional velocity models. *Stud. Geophys. Geod.*

Wang, Z., Zhao, D., Liu, X., Chen, C., & Li, X. (2017). *P* and *S* wave attenuation tomography of the Japan subduction zone. *Geochemistry, Geophysics, Geosystems, 18*(4), 1688-1710.

Yang, X., Bondár, I., McLaughlin, K., & North, R. (2001). Source specific station corrections for regional phases at Fennoscandian stations. *Pure and Applied Geophysics*, 35-57.

Zhao, D. (2012). Tomography and dynamics of Western-Pacific subduction zones. *Monogr. Environ. Earth Planets, 1*(1), 1-70.

Zhao, D., Hasegawa, A., & Horiuchi, S. (1992). Tomographic imaging of *P* and *S wave* velocity structure beneath northeastern Japan. *Journal of Geophysical Research, 97*(B13), 19909-19928.

Zhao, D., & Lei, J. (2004). Seismic ray path variations in a 3D global velocity model. *Physics of the Earth Planetary Interiors, 141*(3), 153-166.